Impact of ZrO2 Additive on Microstructure, Magnetic Properties, and Temperature Dependence of the Initial Permeability of LiTiZn Ferrite Ceramics

Andrey Malyshev (malyshev@tpu.ru)
Nacional'nyj issledovatel'skij Tomskij politehniceskij universitet https://orcid.org/0000-0003-0274-6052

Anna B. Petrova
Tomsk Polytechnic University: Nacional'nyj issledovatel'skij Tomskij politehniceskij universitet

Anatoly P. Surzhikov
Tomsk Polytechnic University: Nacional'nyj issledovatel'skij Tomskij politehniceskij universitet

Research Article

Keywords: LiTiZn ferrite ceramics, ZrO2 additive, initial permeability, defect structure

Posted Date: February 23rd, 2021

DOI: https://doi.org/10.21203/rs.3.rs-225375/v1

Impact of ZrO_2 additive on microstructure, magnetic properties, and temperature dependence of the initial permeability of LiTiZn ferrite ceramics

A.V. Malyshev[*1], A.B. Petrova[1], A.P. Surzhikov[1]

[1]Tomsk Polytechnic University, Lenina Avenue 30, 634050 Tomsk, Russia

Abstract

The effect of the diamagnetic ZrO_2 addition on the microstructure and magnetic properties of LiTiZn ferrite ceramics, including the shape and parameters of the temperature dependence of the initial permeability, has been investigated. The defect structure of ferrite ceramic samples is assessed according to our earlier proposed method based on mathematical treatment of the experimental temperature dependencies of the initial permeability. The method is recommended for defects monitoring of soft ferrite ceramics and ferrite products. It was found that the defect structure of ferrite ceramics increased by 350% with an increase in the concentration of the ZrO_2 additive in the range of (0–0.5) wt.%. In this case, for the same samples, the increase in the true physical broadening of reflections is only 20%, and the coercive force by 50%. Simultaneously, the maximum of the experimental temperature dependence of the initial permeability dropped by 45%. The microstructure of all samples is characterized with a similar average grain size according to the SEM data. However, samples with the 0.5wt.% of ZrO_2 are characterized by the formation of conglomerates. A linear relationship was obtained between the defect structure and the width of the reflections, which indicates that this parameter is related to the elastic stress of ferrite ceramics.

Keywords: LiTiZn ferrite ceramics; ZrO_2 additive; initial permeability; defect structure

---

* Corresponding author at: E-mail address: malyshev@tpu.ru (A.V. Malyshev) https://orcid.org/0000-0003-0274-6052

1. Introduction

LiTiZn ferrite ceramics are widely used in microwave devices due to their low costs and excellent ferromagnetic properties with high values of saturation magnetization and Curie point. Such materials have low microwave dielectric loss. Due to the successful combination of electromagnetic properties, such ceramics are used in the production of such microwave devices as phase shifters, isolators, and microwave absorbers.

It is known that defects in the crystal structure of ferrite materials largely determine the properties of ferrite products obtained by various production methods. It is the manufacturing stage that determines, in the main, the defect structure of various ferrite products. Consequently, the development of modes for the ferrites production with the possibility of varying both the chemical composition and the defect structure of the material is an urgent problem of ferrite material science.

Currently, new technologies and chemical methods for producing ferrite materials with high homogeneity of characteristics, low structural defects, nano-sized, and improved and stable performance characteristics prevail in the ferrite material science. Lithium ferrites are usually obtained by the ceramic method of double sintering, where in the first stage, solid-state reactions are carried out between oxides and/or carbonates followed by high-temperature sintering in the second stage [1-3]. High synthesis temperatures lead to the volatility of lithium and oxygen at temperatures above 1000 °C resulting in the magnetic properties deterioration, and dielectric losses increasing in ferrite ceramics [4]. Several wet chemical methods, including self-combustion [5, 6], hydrothermal ball milling [7-9], the method of citrate precursor [10], and sol-gel synthesis [11, 12], have been developed. These methods are utilized to obtain lithium ferrite at lower temperatures, as well as to minimize side phase inclusions and defects featured to ceramic technology.

Also known as the method of solid-phase synthesis using low-melting additives, such as V_2O_5, Bi_2O_3, Al_2O_3 [13-16]. The efficiency of solid-phase synthesis can be increased with using specific methods that allow reagents to be activated directly during the synthesis. It was shown in

[17, 18] that the intense electron beam heating of precursors is an effective method for intensifying solid-state reactions. The radiation-thermal (RT) method combines the simultaneous effects of thermal and radiation factors. Recently, the RT method has been successfully used in the synthesis of some ferrite systems, such as NiZn ferrites [19], hexaferrites [20], and strontium ferrites [21].

Defect structure of ferrite ceramics includes intragranular defects of the conjugation of grain boundaries and crystal lattice defects. Various types of defects and phase inclusions appear when sintering ferrite ceramics using ceramic technology [22, 23]. It is obvious that such defects, along with intragranular porosity, inhibit domain walls and, ultimately, worsen the electromagnetic properties of ferrite ceramics. The latter is determined not only by the chemical composition of the material but also by the content and distribution of defects in it. Thus, in the production of ferrite materials, it is important to know the relationship between defects and magnetic properties.

Earlier, we proposed a method for assessing the defect structure based on the temperature dependence of the initial permeability μ_i. This method has shown its relatively high sensitivity in comparison with the known magnetic control methods, as well as XRD [24].

The parameter μ_i is measured in very weak magnetic fields. Therefore, maximum possible number of defects of various types participate during the deceleration of domain walls motion. Measurements of the structure-sensitive parameter μ_i in a wide temperature range, including the Curie point, at which the magnetic domains are destroyed, make it possible to track changes in the defect structure in ferrite ceramics by changing the shape of the curve. The defect structure was calculated for each temperature curve as a result of mathematical processing using a phenomenological expression [24]. Using model samples doped with the Al_2O_3, it was shown that this diamagnetic addition significantly affects the shape of the temperature curve μ_i. Thus, the possibility of monitoring non-magnetic impurities in ferrite products was shown. However, the question of the universality of this technique remained open. In this work, we study the nature of the influence of another diamagnetic additive – ZrO_2 on the change in the shape of the temperature dependence μ_i.

2. Experimental

2.1. Materials

The industrial ferrite powder, synthesized by oxide technology from a mechanical mixture of oxides and carbonates, was used to prepare the samples. The mixture composition (wt. %): Li_2CO_3 – 11.2; TiO_2 – 18.65; ZnO – 7.6; $MnCO_3$ – 2.74; Fe_2O_3 – 59.81. Suspension of a Bi_2O_3 solution in concentrated nitric acid of 0.22 wt. % was added and was mixed in a ball mill for 4 hours [24].

Toroidal samples with dimensions 18*14*2 mm^3 were sintered under laboratory conditions. We had explored ferrite samples without additives (no additives) and samples with ZrO_2 additives of 0.1, 0.25, 0.5 wt. %. Such an additive is often used to modify the electro physical properties of materials.

Ferrite samples with concentration ZrO_2 additives of 0.75, and 1 wt. % were distinguished by the Curie point (refer 3.1) and hence by their chemical composition. Therefore, such samples were not suitable for a correct comparative study and the following results given only for 4 types of samples: no additives, with a ZrO_2 additive concentration of 0.1, 0.25 and 0.5 wt. %.

Sintering of samples was carried out in the air under laboratory conditions at a temperature of 1010 °C for 2 h.

2.2 Characterization techniques

The Curie point $T_{C\ DTG}$ were determined by the thermomagnetometric method on an STA 449C Jupiter thermal analyzer (Netzsch, Germany) [25]. The TG and DTG curves were obtained in the heating mode at a rate of 50 deg/min in a constant magnetic field of about 5 Oe.

We used hydraulic press PGr-10 for compaction of toroidal samples [24].

The diffractograms were obtained using an ARL X'TRA X-ray diffractometer, Cuk□ radiation. Scanning angles 2θ = (10 – 80) degrees with a scan rate of 0.01°/s. The phase compositions of the examined samples were determined using the PDF-4 powder data base of the International Centre for Diffraction Data (ICDD). PDF card 04-020-6937. The XRD patterns were processed by the full-profile Rietveld analysis using the Powder Cell 2.5 software.

Williamson-Hall's formula [26]

$$\beta^2 = \lambda / (D_c \cdot \cos(\theta))^2 + 4 \cdot \varepsilon \cdot tg(\theta)^2 \quad (1)$$

Where β – physical broadening of the diffraction maximum;

λ – radiation wavelength;

D_c – coherent scattering region (crystallite size);

θ – Bragg reflection angle;

ε - strains of the crystal lattice.

The parameters of the magnetic hysteresis loop were measured using an oscillographic circuit (based on a Tektronix-2012B two-channel oscilloscope) [24].

Electronic images were obtained on a Hitachi TM-3000 scanning electron microscope on polished and chemically etched transverse cleavages of the samples. The average grain size (D) was calculated by the intercept method.

The technique for measuring inductance using an automatic bridge meter is given in [24, 27]. The measurement was carried out on an E4960AL low-frequency meter in an electromagnetic field with a frequency of 1 kHz and a low strength of 8 A/m.

The initial permeability (μ_i) of the toroidal ferrite samples was calculated by using the formula (2) [22].

$$\mu_i = \frac{L \cdot 10^7}{2 \cdot h \cdot N^2 ln(D/d)} \quad (2)$$

L – the induction of coil (H);

N – number of turns;

h – toroid height (m);

D/d – toroid outside/inside diameter (m).

3. Results and discussion

3.1 Thermomagnetometric measurements

The results of thermomagnetometric measurements (Fig. 1) showed that the Curie points $T_{C\,DTG}$ for samples of LiTiZn ferrite ceramics with 0.75 and 1 wt.% of ZrO_2 differ significantly (on 6 – 8 degrees) from the Curie points for samples without or containing 0.1, 0.25 or 0.5 wt.% of ZrO_2. Such changes may indicate an alteration in the chemical composition of the ferrite.

We emphasize, that ferrite samples with diamagnetic ZrO_2 additive concentrations 0.75 and 1 wt.% were not suitable for correct comparative study. Therefore, the experimental results of this investigation given only for 4 types of samples: no additives, with a ZrO_2 additive concentration of 0.1, 0.25 and 0.5 wt. %.

3.2 X-ray diffraction analysis

Fig. 2 shows diffractograms for model samples of LiTiZn ferrite ceramics. The scale is the same for both 2θ and intensity.

Table 1 show that the addition of ZrO_2 has a weak effect on the X-ray structural parameters of the ferrite ceramics. With an increase in the concentration of ZrO_2, the lattice parameter and crystallite size (Coherent scattering regions) slightly decrease. In this case, the micro-strain is practically independent of this parameter. Emphasize that the nature of the effect of ZrO_2 additive on the X-ray structural parameters differs significantly from the previously discovered effect of Al_2O_3 additive on ferrite ceramics of the same composition [27].

Table 1

Effect of ZrO_2 additive on the X-ray structural parameters of LiTiZn ferrites

Samples type	Lattice parameter (nm)	Micro-strain·10^4	Crystallite size (nm)
No additive	0.8367	4	93
Add. 0.1%	0.8366	4	88
Add. 0.25%	0.8364	5	86
Add. 0.5%	0.8363	5	86

3.3 Morphological analysis

Fig. 3 shows electron micrographs of LiTiZn ferrite ceramic samples.

The average grain size calculated by the intercept method differs slightly for different samples D = (7.1 ± 0.4) μm. The samples with addition of 0.5 wt.% ZrO_2 are characterized by the formation of agglomerates. As can be seen from Fig. 3, all samples have a polycrystalline structure with formed grain boundaries. Obviously, the white intergranular inclusions correspond to Bi_2O_3 added during the synthesis of industrial ferrite powder. Such behavior can also be caused by ZrO_2 additives.

3.4 Temperature dependencies of the initial permeability

Fig. 4 shows impact of ZrO_2 additive on the temperature dependencies of the initial permeability for LiTiZn ferrite ceramic samples.

The mathematical treatment of the temperature dependencies of initial permeability was carried out using the phenomenological expression (3) proposed in [24]. As a result, the calculated values of the main parameters of the phenomenological expression, including the Curie point (T_c), the defect structure (β/α) were obtained. Table 2 shows the calculated main parameters of the phenomenological expression, as well as the parameters of the temperature curves.

$$\mu_i = \frac{1+x}{1+N\cdot x}, \qquad x=\left[\frac{\left(1-\frac{T}{T_c}\right)^{\delta}}{\alpha\left(1-\frac{T}{T_c}\right)^{\gamma}+\beta}\right]^{g} \tag{3}$$

The coefficients a, b, g and d are determined by the relations (4), (5), (6):

$$\alpha = \frac{K_1(T)}{M_s^r(T)}, \quad \beta = \frac{\lambda_s(T)}{M_s^r(T)}\cdot\sigma, \delta = (r-n)f, \gamma = (m-n)f \tag{4}$$

$$\frac{K_1(T)}{K_1(0)} = \left[\frac{M_s(T)}{M_s(0)}\right]^m, \quad \frac{\lambda_s(T)}{\lambda_s(0)} = \left[\frac{M_s(T)}{M_s(0)}\right]^n \tag{5}$$

$$M_s(T) = M_s(0)\left[1-\frac{T}{T_c}\right]^f \tag{6}$$

Where g=2 and r=2 – exponent of power in (3), (4) for model of initial permeability by Smith and Wijn;

m, n , f – exponent of power in (5), (6);

K_1 – crystallographic magnetic anisotropy;

l_s – magnetostriction constant;

σ – average elastic stresses;

N – the magnitude of the demagnetizing factor;

M_s – saturation magnetization;

T_c – Curie point.

Table 2

Impact of ZrO_2 additive on the parameters of temperature dependence of initial permeability

Samples type	N $\cdot 10^3$	T_c (°C)	μ_{max}	T_m (°C)	$\beta/\alpha\ 10^3$
No additive	1.79 ±0.03	269.2 ±0.3	430.8	242.5	4.88
Add. 0.1%	2.34 ±0.05	264.7±0.3	374	232.9	6.22
Add. 0.25%	2.05±0.06	265.6±0.3	358.2	229.5	10.52
Add. 0.5%	1.34 ±0.03	265.3 ±0.2	230.2	240.8	22

Where N – demagnetization coefficient;

μ_{max} –maximum of temperature dependence of initial permeability;

T_m – position of a peak of the temperature dependence of the initial permeability on the temperature scale;

β/α – defect structure of ferrite ceramic samples.

From the data in Table 2, it follows that with an increase in the ZrO_2 concentration up to 0.5 wt.% the defect structure β/α of ferrite ceramics increased by 350 %. At the same, the maximum of the temperature dependence of μ_i dropped by 45%. The other parameters do not change significantly with an increase in the ZrO_2 additive concentration. Compared to the results of the Al_2O_3 adding to LiTiZn ferrite, the ZrO_2 addition also causes a similar increase in the defect structure β/α and a reduction of μ_{max}, but the character of the change in the position of the peak on the temperature scale T_m is different [27]. As it can be seen from the Table 2, the T_m first falls with an increase in the ZrO_2 concentration up to 0.25 wt.% (shifts from the Curie point), and then sharply increases (a jump to the Curie point) with an increase in the ZrO_2 concentration to 0.5 wt.%. Also, the demagnetizing factor does not increase monotonically with an increase in the Al_2O_3 concentration but passes through a maximum at a ZrO_2 concentration of 0.1 wt.%. The Curie point increases by more than 10 degrees if the ZrO_2 concentration is 0.75 wt.% and above. This indicates the effect of additives on the chemical composition of ferrites [27].

In [28] for NiCuZn ferrites, a decrease in the maximum of the temperature dependence μ_i with an increase in the concentration of Al_2O_3 was found. The authors attribute this behavior to the influence of additives on the domain walls motion. Therefore, the behavior of μ_{max} described above can be used to estimate the defect structure or diamagnetic impurities in ferrite ceramics.

Fig. 4 shows that the concentration of ZrO_2 affects the character of changes in the experimental temperature dependence of the initial permeability. With an increase in the concentration of ZrO_2 up to 0.25 wt.%, a shift of the maximum of this dependence on the Curie point is observed. However, with an increase in the ZrO_2 concentration to 0.5 wt.%, the maximum

shifts to the Curie point. We emphasize that in the case of Al_2O_3 adding, a different character of the temperature dependence transformation is observed, at which maximum with an increase in concentration to 0.5 wt.% shifts monotonically from the Curie point. In the case of both types of additives, a similar decrease in the maxima of the experimental temperature dependencies with an increase in the concentration of diamagnetic additives is observed [27].

3.5 Magnetic analysis

Fig. 5 shows the impact of diamagnetic ZrO_2 addition on the magnetic hysteresis loop parameters (Table 3). The magnetizing field is selected based on the saturation of the dependence of the maximum induction on the magnetic field strength $B_m(H)$. The introduction of ZrO_2 affects the residual induction B_r, the maximum induction B_m and the coercive force H_c.

Table 3

Parameters of the hysteresis loop of LiTiZn ferrite ceramic samples with ZrO_2 additive

Samples type	B_s (mT)	B_r (mT)	H_c (A/m)
No additive	155.7	128.8	78.3
Add. 0.1%	145.6	121.6	79.8
Add. 0.25%	151	125	84.7
Add. 0.5%	143	120	119.6

Where B_r – residual induction; B_m – the maximum induction; H_c – the coercive force.

It follows from Table 3 that B_r and B_s decrease monotonically, while H_c increases with increasing concentration of ZrO_2. This behavior is due to the appearance and growth of demagnetizing fields associated with the action of elastic stress fields. With an increase in ZrO_2 to 0.5%, H_c increases by 50%.

3.6 The true physical broadening

The true physical broadening δ was determined for the same samples. The widths of the diffraction reflections from the (400) and (800) planes were determined, considering the doublet spectral line by the method of decomposition into Gaussian components [24].

According to the data in Table 4, with an increase in the concentration of ZrO_2 to 0.5%, the true physical broadening increases by 20%. A similar behavior is observed for the (800) reflection.

Table 4

True physical broadening δ for reflex (400)

Samples type	W (degree)	δ (degree)
Standard	0.083	-
No additive	0.158	0.134
Add. 0.1 %	0.163	0.14
Add. 0.25 %	0.174	0.153
Add. 0.5 %	0.181	0.161

Here W – peak width at half height.

Comparing the data in Table 2 with the data in Tables 3 and 4, it follows that H_c increases by 50%, and true physical broadening δ - by 20% only while the concentration of the ZrO_2 increase to 0.5 %. At the same time, the defect structure β/□, determined from the temperature dependence of □ᵢ increases by 350 %. Consequently, our earlier proposed method for determining the defect structure with mathematical analysis of the temperature dependencies of □ᵢ significantly exceeds the sensitivity of typical magnetic and X-ray methods [24].

The obtained results showed that the ZrO_2 diamagnetic addition degrades some magnetic parameters of model samples of LiTiZn ferrite. Such behavior is typical for magnetic dilution of ferrimagnetic materials [22]. The main idea of this study was to test a new method for calculating the defect structure using model samples containing a controlled amount of a diamagnetic additive. Also, the comparison with the known methods of defect control for the same samples was made.

3.7 The defect structure and elastic stress

It is known that the width of X-ray reflections is determined, in turn, by elastic stresses in the material [29]. In this regard, it is interesting to establish the relationship between elastic stresses in the material and the defect structure □□□. Fig. 6 shows the dependence between the width of the (400) reflection and the defect structure □□□ for LiTiZn ferrite ceramic samples with the addition of ZrO_2. Fig. 7 shows the dependence between the width of the (400) reflection and the ZrO_2 additive concentration.

The appearance of elastic stress of ferrite connected with baking the ZrO_2 oxide particles with the ferrite matrix grains and the difference in the thermal expansion coefficients, the lattice structure of both phases. In this case, the residual stresses can be estimated according to the scheme proposed in [30]. At low concentrations of inclusions, the overlap of the elastic stress fields can be neglected, and in this case, the volume of the sample that has experienced strain will be proportional to the amount of the additive. Such behavior is observed on the studied model ferrite ceramics samples (Fig. 6 and Fig. 7).

Obviously, Fig. 6 and Fig.7 shows a close to a linear relationship between the reflection width and the defect structure □□□□and ZrO_2 additive concentration. Consequently, parameter □□□□can also be used to characterize elastic stresses in ferrite ceramics [24]. As a result, it was shown that an increase in elastic stresses in LiTiZn ferrite ceramics is caused by the introduction of diamagnetic ZrO_2 into the material. In this case, the elastic stresses of the model samples of ferrite ceramics are

proportional to the defect structure □□□, determined from the temperature dependence of initial permeability.

4. Conclusion

The previously proposed method for determining the defect structure of LiTiZn ferrite ceramic samples with ZrO_2 diamagnetic additive has been tested.

The high sensitivity of the method, in comparison with typical magnetic methods and XRD, was shown. Even the initial concentrations of the ZrO_2 diamagnetic additive (0.1 – 0.5 wt.%) affect the parameters of temperature dependencies of initial permeability and the calculated defect structure. Therefore, the method is recommended for defects monitoring of soft ferrite ceramics and ferrite products.

It is shown that the defect structure of ferrite ceramics can be estimated from the maximum of this temperature dependence of the initial permeability near the Curie point.

It has been experimentally established that the defect structure is associated with the elastic stress of ferrite ceramics.

Declaration of Competing Interest

The authors declare that they have no known competing financial interests or personal relationships that could have appeared to influence the work reported in this paper.

Acknowledgments

The research is funded from The Ministry of Science and Higher Education of the Russian Federation in part of the science program (project FSWW-2020-0014). The experimental

calculations are carried out at Tomsk Polytechnic University within the framework of Tomsk Polytechnic University Competitiveness Enhancement Program grant.

References

1. P.P. Mohapatra, P. Dobbidi, J. Magn. Magn. Mater. **500** 166354 (2020) https://doi.org/10.1016/j.jmmm.2019.166354
2. J. Li, D. Zhou, J. Alloys Comp. **785** 13–18 (2019) https://doi.org/10.1016/j.jallcom.2019.01.148
3. P.P. Mohapatra, S. Pattipaka, P. Dobbidi, Ceramics Int. **45** 25010–25019 (2019) https://doi.org/10.1016/j.ceramint.2019.04.040
4. L. Jia, Y. Zhao, F. Xie, Q. Li, Y. Li, Ch. Liu, H. Zhang, AIP Advances **6** 056214 (2016) https://doi.org/10.1063/1.4943928
5. S.S. Hossain, K. Praveena, P.K. J Mater Sci: Mater Electron 31, 15097–15107 (2020) https://doi.org/10.1007/s10854-020-04074-3
6. B.A. Patil, J.S. Kounsalye, A.V. Humbe et al., J Mater Sci: Mater Electron (2021) https://doi.org/10.1007/s10854-020-05197-3
7. E.N. Lysenko, A.V. Malyshev, V.A. Vlasov, E.V. Nikolaev, A.P. Surzhikov, J. Therm. Anal. Calorim. **134** 127–133 (2018). https://doi.org/10.1007/s10973-018-7549-4
8. W. Chen, W. Wu, C. Zhou et al., Journal of Elec Materi **47,** 2110–2119 (2018) https://doi.org/10.1007/s11664-017-6021-8
9. X. Wu, W. Chen, W. Wu et al., J Mater Sci: Mater Electron **28,** 18815–18824 (2017) https://doi.org/10.1007/s10854-017-7831-4
10. M.V. Santhosh Kumar, G.J. Shankarmurthy, E. Melagiriyappa et al., J Mater Sci: Mater Electron **29,** 12795–12803 (2018) https://doi.org/10.1007/s10854-018-9398-0
11. M.G. El-Shaarawy, M.M. Rashad, N.M. Shash et al., J Mater Sci: Mater Electron **26,** 6040–6050 (2015) https://doi.org/10.1007/s10854-015-3181-2
12. M. Irfan, M. Usman, A. Elahi et al., J Mater Sci: Mater Electron **27,** 3637–3644 (2016) https://doi.org/10.1007/s10854-015-4202-x
13. F. Xu, X. Shi, Y. Liao, J. Li, J. Hu, Ceramics Int. **46** 14669–14673 (2020) https://doi.org/10.1016/j.ceramint.2020.02.268.
14. T. Zhou, H. Zhang, Ch. Liu, L. Jin, F. Xu, Y. Liao, N. Jia, Y. Wang, G. Gan, H. Su, L. Jia, Ceramics Int. **42** 16198–16204 (2016) https://doi.org/10.1016/j.ceramint.2016.07.141.

15. Y. Liao, Y. Wang, Zh. Chen, X. Wang, J. Li, R. Guo, Ch. Liu, G. Gan, G. Wang, Y. Li, H. Zhang, Ceramics Int. **46** 487–492 (2020) https://doi.org/10.1016/j.ceramint.2019.08.286
16. F. Xie, L. Jia, Y. Zhao, J. Li, T. Zhou, Y. Liao, H. Zhang, J. Alloys Comp. **695** 3233–3238 (2017) https://doi.org/10.1016/j.jallcom.2016.11.266
17. V.V. Boldyrev, A.P. Voronin, O.S. Gribkov, E.V. Tkachenko, G.R. Karagedov, B.I. Yakobson, V.L. Auslender, J. Solid State Ion. **36** 1–6 (1989) https://doi.org/10.1016/0167-2738(89)90051-9
18. V.L. Auslender, I.G. Bochkarev, V.V. Boldyrev, N.Z. Lyakhov, A.P. Voronin, Electron beam induced diffusion controlled reaction in solids, J. Solid State Ion. **101-103** 489–493 (1997) https://doi.org/10.1016/S0167-2738(97)84073-8
19. V.G. Kostishin, V.V. Korovushkin, A.G. Nalogin, S.V. Shcherbakov, I.M. Isaev, A.A. Alekseev, A.Y. Mironovich, D.V. Salogub, Phys. Solid State **62** 1156–1164 (2020) https://doi.org/10.1134/S1063783420070124
20. E.P. Naiden, V.A. Zhuravlev, R.V. Minin, V.I. Suslyaev, V.I. Itin, E.Yu. Korovin, Int. J Self-Propag. High-Temp. Synth. **24** 148–151 (2015) https://doi.org/10.3103/S1061386215030073
21. U.V. Ancharova, M.A. Mikhailenko, B.P. Tolochko, N.Z. Lyakhov, M.V. Korobeinikov, A.A. Bryazgin, Z.S. Vinokurov, A.G. Selyutin, IOP Conf. Ser.: Mater. Sci. Eng. **110** 012110 (2016) https://doi.org/10.1088/1757-899X/110/1/012110
22. J. Smith, H.P.J. Wijn, Ferrites: Physical Properties of Ferromagnetic Oxides in Relation to Their Technical Application (Phillips Technical Library, Eindhoven, 1959), pp. 233.
23. T. Zheng, J. Wu, Scripta Materialia **187** 418–423 (2020) https://doi.org/10.1016/j.scriptamat.2020.06.063
24. A.V. Malyshev, A.B. Petrova, A.N. Sokolovskiy, A.P. Surzhikov, J. Magn. Magn. Mater. **456** 186–193 (2018) https://doi.org/10.1016/j.jmmm.2018.02.032
25. P.K. Gallagher, J. Therm. Anal. Calorim. **49** 33–44 (1997) https://doi.org/10.1007/BF01987419
26. G.K. Williamson, W.M. Hall, Acta Metall. **1** 22–31 (1953)
27. A.V. Malyshev, A.B. Petrova, A.P. Surzhikov, Ceramics Int. **44** 20749–20754 (2018) https://doi.org/10.1016/j.ceramint.2018.08.073
28. S. Takane, H. Umeda, T. Aoki, T. Murase, Key Eng. Mater. **485** 225–228 (2011) https://doi.org/10.4028/www.scientific.net/KEM.485.225

29. R.E. Dinnebier, S.J.L. Billinge, Powder Diffraction: Theory and practice (the Royal Society of Chemistry, Cambridge, 2008), pp. 51–68 https://doi.org/10.1107/S010876730802850X
30. J. Selsig, J. Amer. Ceram. Soc. **44** 419–422 (1961)

Figure Captions

Fig. 1 TG and DTG curves obtained for of LiTiZn ferrite ceramic samples: (a) no additives; (b) 0.75% of ZrO_2; (c) 1% of ZrO_2

Fig. 2 X-ray diffraction patterns of LiTiZn ferrite samples: (a) no additives; (b) 0.1% of ZrO_2; (c) 0.25% of ZrO_2; (d) 0.5% of ZrO_2

Fig. 3 Electron micrographs of LiTiZn ferrite ceramic samples: (a) no additives; (b) 0.1% of ZrO_2; (c) 0.25% of ZrO_2; (d) 0.5% of ZrO_2

Fig. 4 Temperature dependencies of the initial permeability of LiTiZn ferrite ceramic samples: (a) no additives; (b) 0.1% of ZrO_2; (c) 0.25% of ZrO_2; (d) 0.5% of ZrO_2. Symbols – experimental data, solid lines – calculated curves

Fig. 5 Hysteresis loops for LiTiZn ferrite ceramic samples: (a) no additives; (b) 0.1% of ZrO_2; (c) 0.25% of ZrO_2; (d) 0.5% of ZrO_2

Fig. 6 Dependence of the width of the (400) reflection on the defect structure □□□ of model samples. The solid line is the approximation straight line

Figures

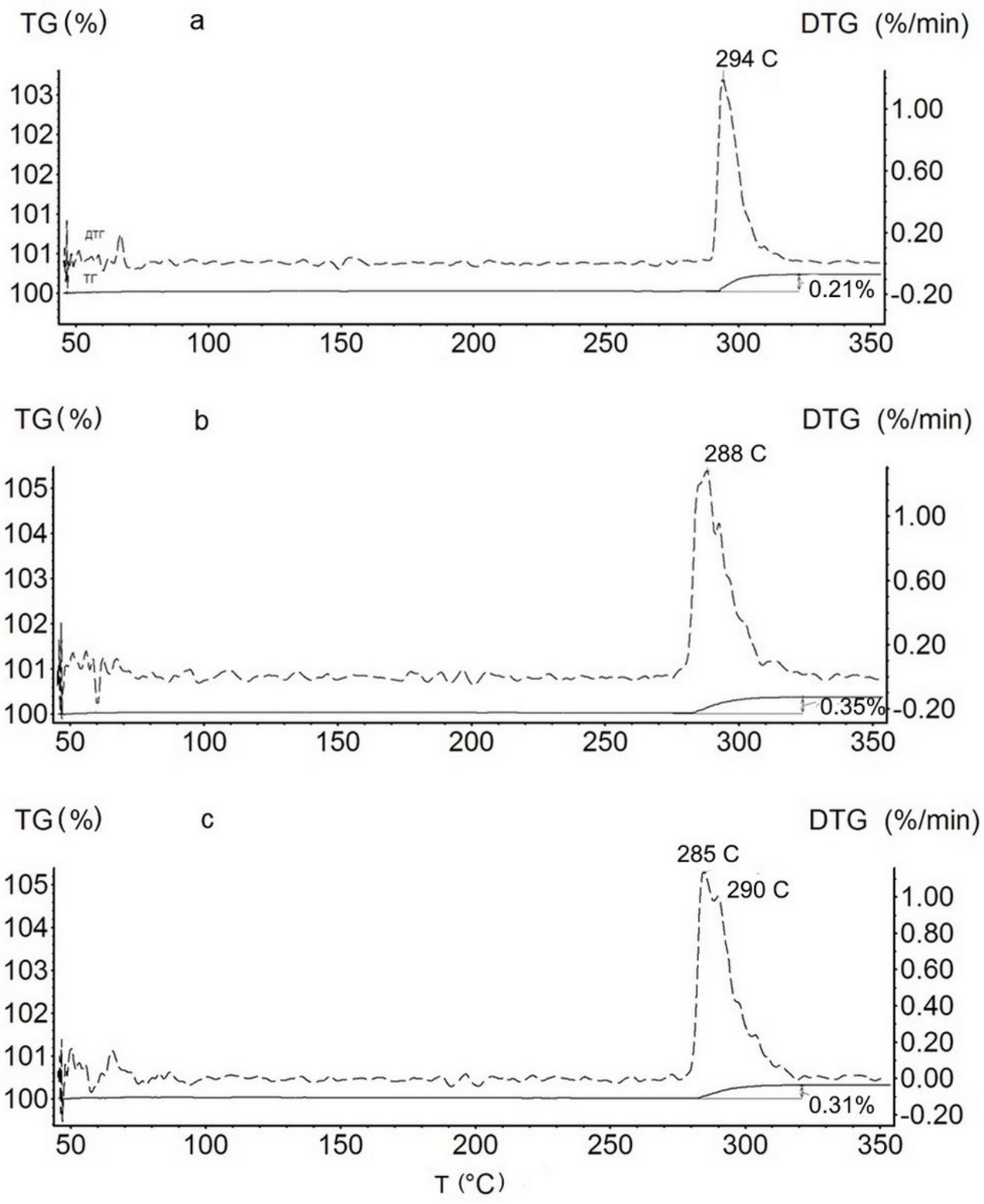

Figure 1

TG and DTG curves obtained for of LiTiZn ferrite ceramic samples: (a) no additives; (b) 0.75% of ZrO2; (c) 1% of ZrO2

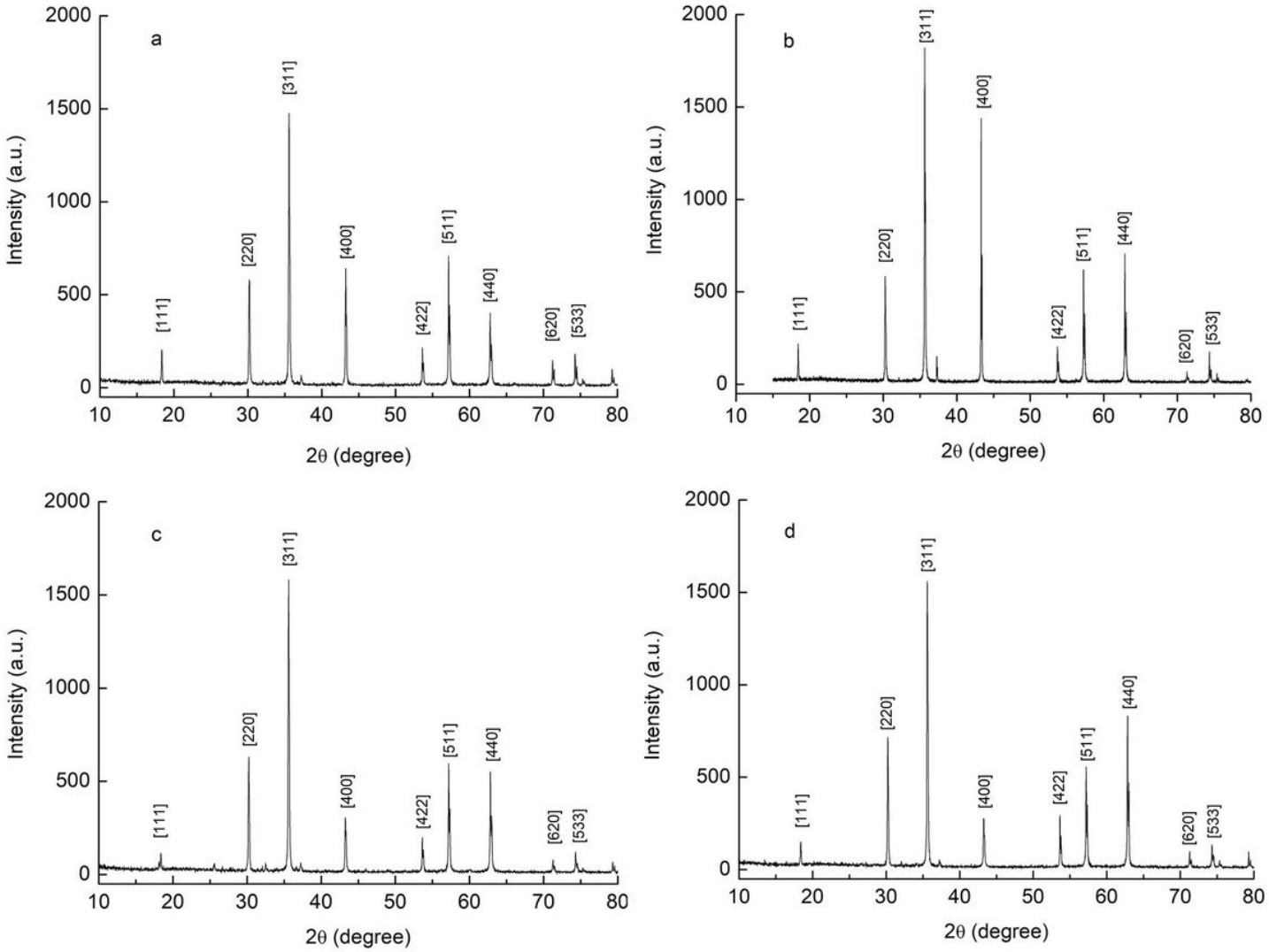

Figure 2

TG and DTG curves obtained for of LiTiZn ferrite ceramic samples: (a) no additives; (b) 0.75% of ZrO2; (c) 1% of ZrO2

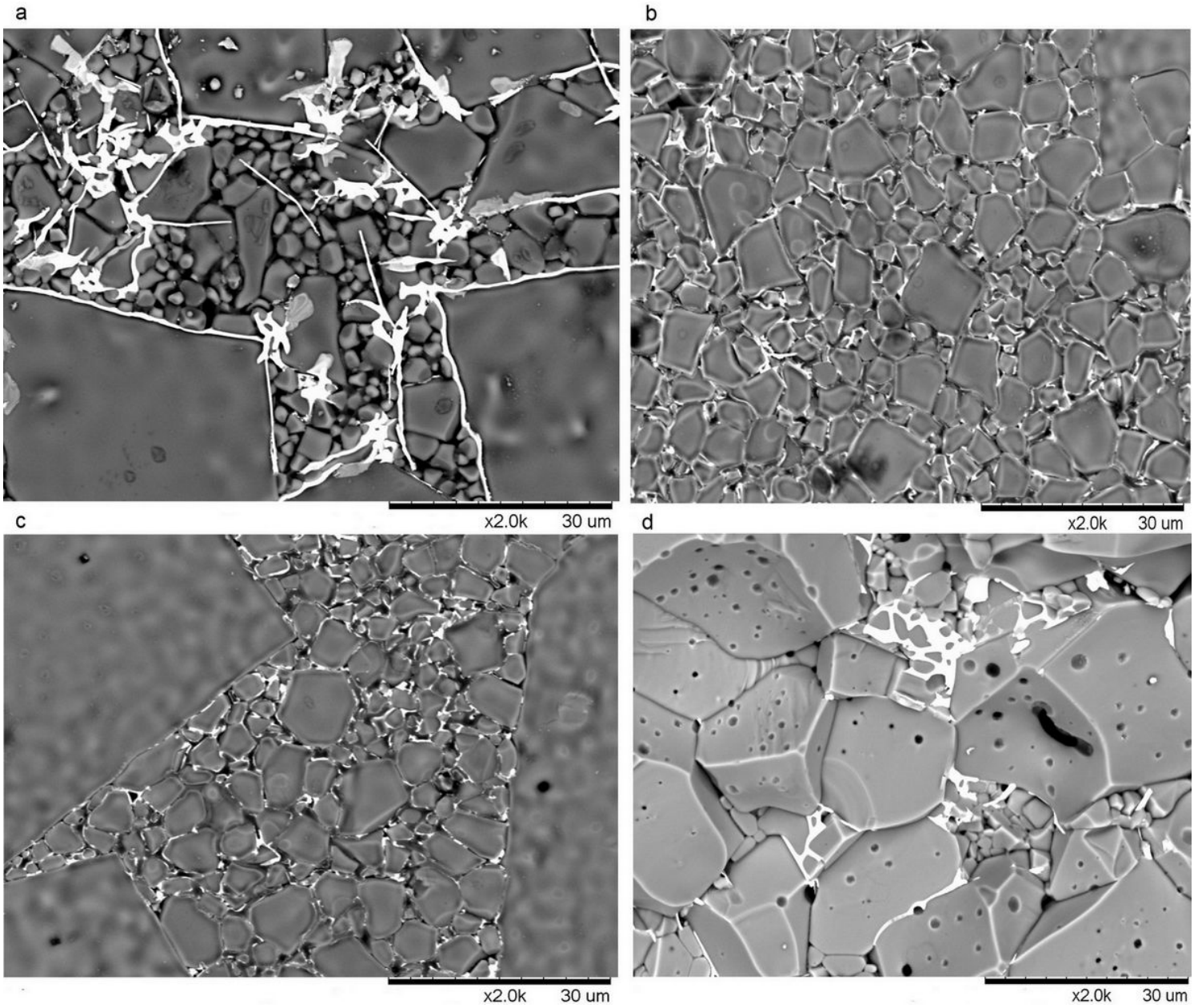

Figure 3

Electron micrographs of LiTiZn ferrite ceramic samples: (a) no additives; (b) 0.1% of ZrO2; (c) 0.25% of ZrO2; (d) 0.5% of ZrO2

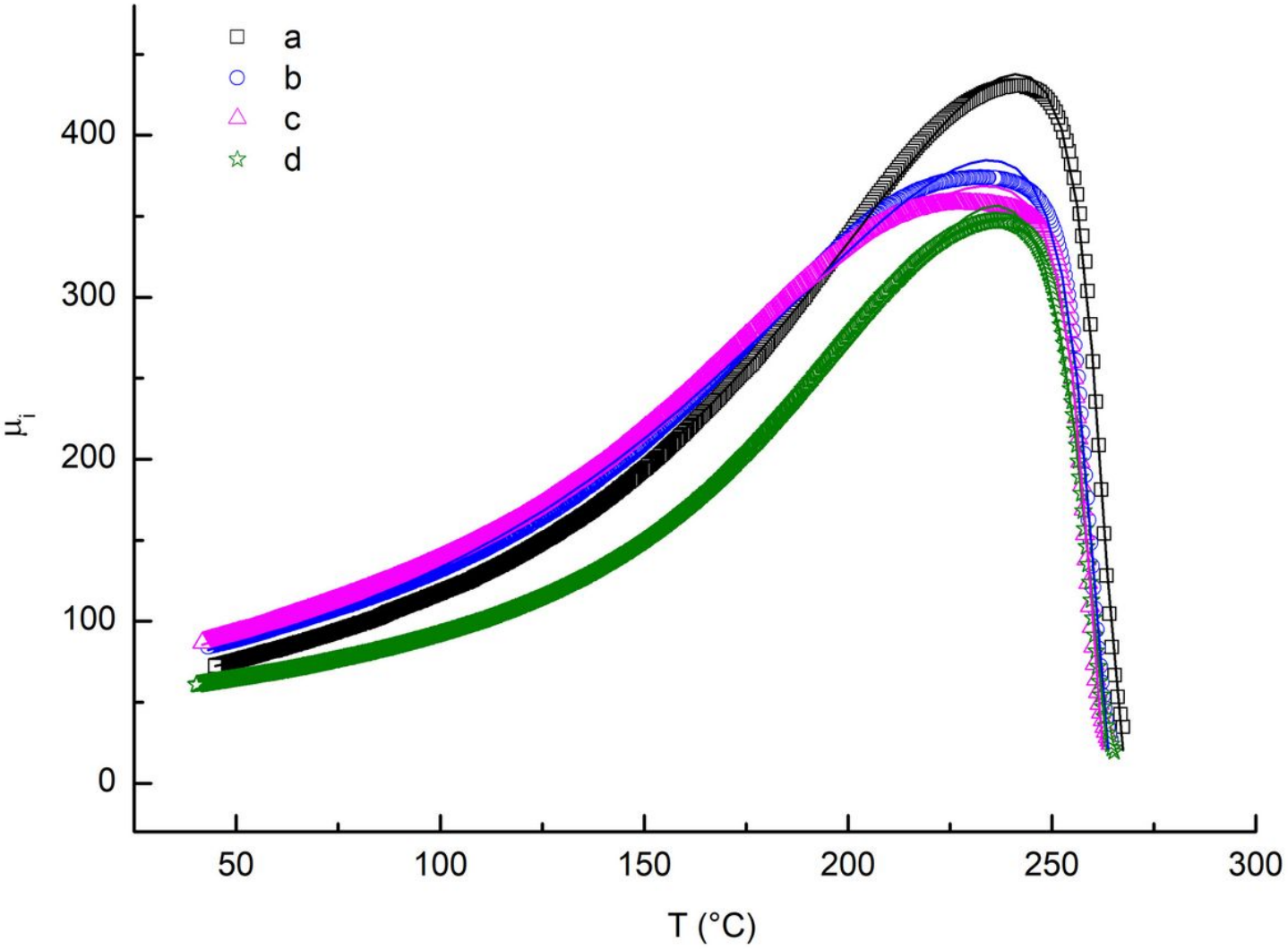

Figure 4

Temperature dependencies of the initial permeability of LiTiZn ferrite ceramic samples: (a) no additives; (b) 0.1% of ZrO2; (c) 0.25% of ZrO2; (d) 0.5% of ZrO2. Symbols – experimental data, solid lines – calculated curves

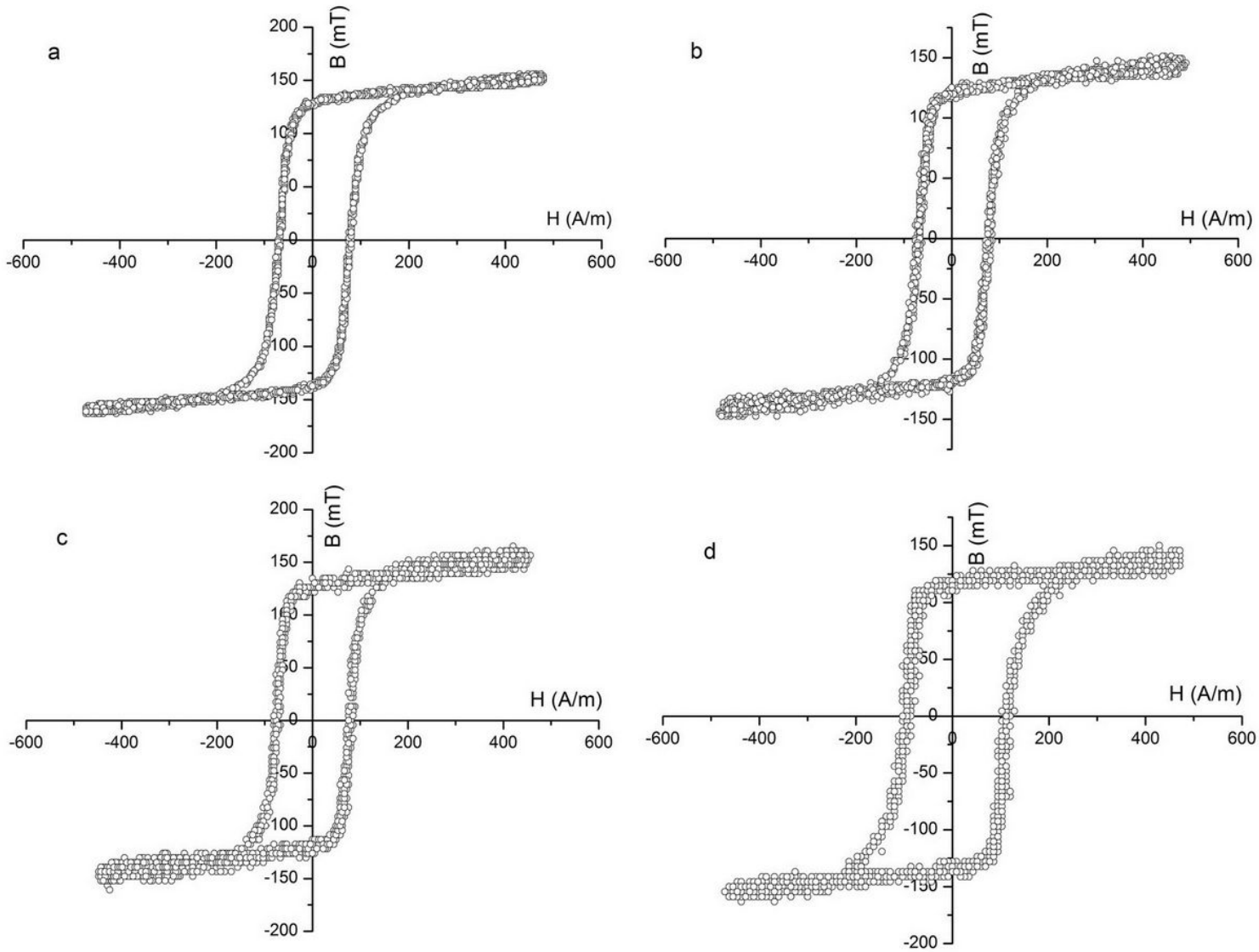

Figure 5

Hysteresis loops for LiTiZn ferrite ceramic samples: (a) no additives; (b) 0.1% of ZrO2; (c) 0.25% of ZrO2; (d) 0.5% of ZrO2

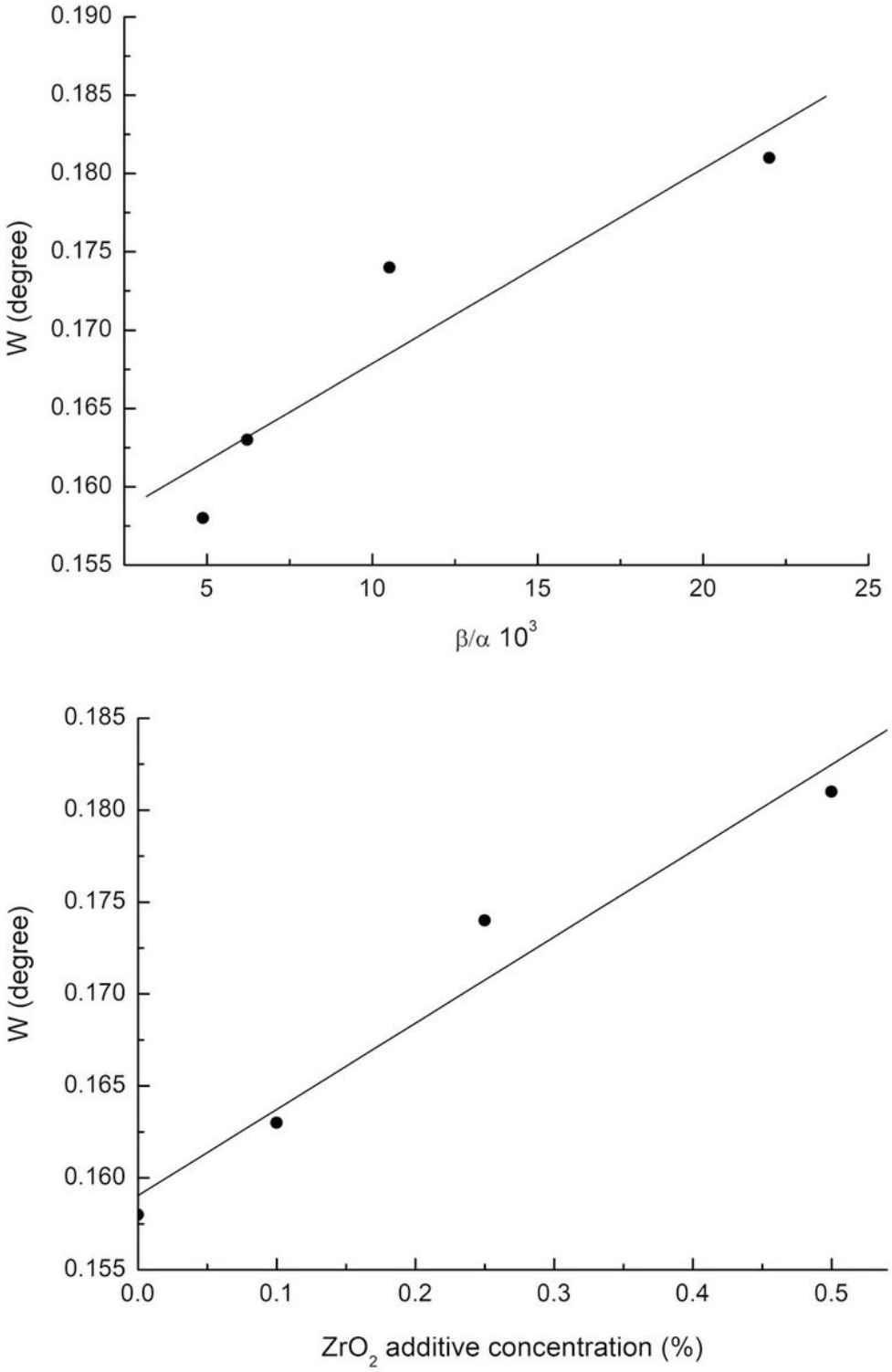

Figure 6

Dependence of the width of the (400) reflection on the defect structure β/α of model samples. The solid line is the approximation straight line